Temperature dependent energy relaxation time in AlGaN/AlN/GaN heterostructures

Engin Tiras [a,*], Ozlem Celik [a], Selman Mutlu [a], Sukru Ardali [a], Sefer Bora Lisesivdin [b], Ekmel Ozbay [c,d]

[a] Department of Physics, Faculty of Science, Anadolu University, Yunus Emre Campus, 26470 Eskisehir, Turkey
[b] Department of Physics, Faculty of Science and Arts, Gazi University, Teknikokullar, 06500 Ankara, Turkey
[c] Nanotechnology Research Center, Department of Physics, Bilkent University, 06800 Ankara, Turkey
[d] Department of Electrical and Electronics Engineering, Bilkent University, 06800 Ankara, Turkey

ARTICLE INFO

ABSTRACT

The two-dimensional (2D) electron energy relaxation in $Al_{0.25}Ga_{0.75}N/AlN/GaN$ heterostructures was investigated experimentally by using two experimental techniques; Shubnikov-de Haas (SdH) effect and classical Hall Effect. The electron temperature (T_e) of hot electrons was obtained from the lattice temperature (T_L) and the applied electric field dependencies of the amplitude of SdH oscillations and Hall mobility. The experimental results for the electron temperature dependence of power loss are also compared with the current theoretical models for power loss in 2D semiconductors. The power loss that was determined from the SdH measurements indicates that the energy relaxation of electrons is due to acoustic phonon emission via unscreened piezoelectric interaction. In addition, the power loss from the electrons obtained from Hall mobility for electron temperatures in the range $T_e > 100$ K is associated with optical phonon emission. The temperature dependent energy relaxation time in $Al_{0.25}Ga_{0.75}N/AlN/GaN$ heterostructures that was determined from the power loss data indicates that hot electrons relax spontaneously with MHz to THz emission with increasing temperatures.

© 2012 Elsevier Ltd. All rights reserved.

1. Introduction

Group III-nitride materials are very suitable for applications in high power, high frequency, and high temperature electronics [1]. Most devices are designed to operate under a high electric field.

* Corresponding author.
 E-mail address: etiras@anadolu.edu.tr (E. Tiras).

At a high electric field, the electrons equilibrate at a much higher temperature than the lattice temperature. The determination of the temperature of electrons, under electric-field heating conditions in the steady state, provides useful information about the electron–phonon interactions involved in the energy relaxation process.

At below room temperatures, the contribution to the energy relaxation rates of elastic scattering mechanisms, such as ionized impurity scattering, alloy disorder scattering, and interface roughness scattering, can be neglected [2]. Therefore, inelastic scattering mechanisms should be considered to explain the rise of temperature of the 2D electron gas where the applied electric field causes the heating of electrons. Typically, at temperatures below 30 K, the sources limiting the energy relaxation are the optical phonon energy, plasmon energy, and relative strengths of acoustic phonons. At such low temperatures, longitudinal optical phonon scattering becomes negligible and the main source of energy relaxation is acoustic phonon scattering. In high polar materials, such as GaN, longitudinal optical (LO) energy is considerably high, and LO phonon scattering should be a dominant loss mechanism at electron temperatures of around 100 K and above [3,4]. Therefore, at high temperatures, the optical phonon scattering mechanism should be considered for explaining the rise of temperature of the 2D electron gas where the applied electric field causes the heating of electrons.

The Shubnikov-de Haas (SdH) oscillations in magnetoresistance provide an accurate and sensitive technique that has been employed successfully in the investigations of electron energy relaxation in the acoustic-phonon regime [5–8]. The method is based on the assumption that ionized-impurity scattering, alloy scattering, and interface roughness scattering, which determine the low-temperature transport mobility of electrons, are elastic in nature. Consequently, the energy that is gained by electrons in an applied electric field is dissipated via the emission of acoustic phonons.

In degenerate and non-degenerate material, where the momentum relaxation is dominated by ionized impurity, remote impurity, interface roughness, or optical phonon scattering [3,5,6,9], electron temperatures as a function of the applied electric field can be determined as a function of the applied electric field by a simple comparison of the electric field dependent and lattice temperature dependent mobility curves [5,6,9–11].

In GaN based heterostructures, two-dimensional electron gas (2DEG) is formed at the GaN side of the interface between the barrier and GaN layers. Comparatively little work has been published in the literature concerning measurements of the power loss of hot electrons in material systems, where the 2D electron gas is confined in GaN-based systems. Most reports in the literature obtain hot electron energy relaxation in GaN systems from the analysis of the amplitude variation of quantum oscillations [12–15] and mobility [10,11] with an electric field and temperature, fluctuations in the electron velocities under the high electric field [4,16], and decay of the anti-stokes line intensity [17].

The determination of the fundamental optical and electronic properties is a scientifically technological and fundamental important parameter for designing optoelectronic devices. The energy relaxation time of the hot electron is not yet well-known. In the present paper, the temperature of hot electrons (T_e) of the sample and corresponding power loss (P) have been determined as a function of the applied electric field using both SdH effect and mobility comparison methods in $Al_{0.25}Ga_{0.75}N/AlN/GaN$ heterostructures. The experimental results are compared with a two-dimensional model in the acoustic phonon regime and optical phonon regime. The temperature dependent energy relaxation time in $Al_{0.25}Ga_{0.75}N/AlN/GaN$ heterostructures are also determined from power loss data. The results are discussed in the framework of the current theoretical models concerning carrier energy loss rates in wide bandgap semiconductors.

2. Experimental procedure

The AlGaN/AlN/GaN heterostructure was grown by the metalorganic chemical vapor deposition (MOCVD) technique on a sapphire substrate. The layers consisted of a 320 nm AlN buffer layer, followed by a 1.7 μm undoped GaN layer, a 1 nm AlN spacer layer and a 20 nm $Al_xGa_{1-x}N$ ($x = 0.25$) layer capped with a 3 nm GaN. The $Al_{0.25}Ga_{0.75}N$ layer was doped with Si, at a doping density of 10^{18} cm^{-3}. The 2DEG was formed at the interface between the undoped GaN layer and AlN spacer. The sample was grown in a wurtzite structure. During the growth, the sample parameters, including doping density, alloy fractions, and layer thicknesses, were estimated from the calibrated charts for

the specific growth conditions and materials. After the growth, these parameters were measured for each wafer, using standard characterization techniques such as photoluminescence, scanning transmission electron spectroscopy, capacitance–voltage profiling, and energy dispersive X-ray analysis [18].

The longitudinal resistance (R_{xx}) along the applied current measurements were carried out as functions of: (i) the applied electric field F at a fixed lattice temperature T_{L0}; and (ii) the lattice temperature T_L at a fixed electric field F_0 that was low enough to ensure ohmic conditions and hence to avoid carrier heating. In the experiments, a conventional dc technique in combination with a constant current source (Keithley 2400) and a nanovoltmeter (Keithley 2182A), in a cryogen free superconducting magnet system (Cryogenics Ltd., Model No. J2414), were used. The current (I) flow was in the plane of the electron gas and the current through the sample was kept low enough to ensure ohmic conditions. Steady magnetic fields up to 11 T were applied perpendicular to the plane of the samples and hence to the plane of 2D electron gas. All the measurements were taken in the dark. In order to check the 2D nature of the electron gas giving rise to the quantum oscillations in magnetoresistance, the measurements were also performed as a function of the angle θ between the normal to the plane of the 2D electron gas and the applied magnetic field. It was found that the peak position shift with a factor of $\cos\theta$ and the oscillations disappear at $\theta = 90°$. This observation is a characteristic of 2D electron gas [19].

For the classical low magnetic field temperature dependent Hall Effect measurements, R_{xx} and the Hall resistance (R_{xy}) were measured as a function of temperature from 1.8 to 275 K. A static magnetic field ($B = 1$ T) was applied to the sample perpendicular to the current plane. The dc voltage applied to the sample was kept low enough to ensure ohmic conditions in order to avoid carrier heating.

For the high pulsed I–V measurements, a simple bar geometry with the length $L = 0.6$ mm and width $w = 0.2$ mm was used. Short bias pulses were applied to minimize Joule heating. In the experiments, a conventional pulse technique in combination with a pulse voltage source (Avtech-AVIR-4-B) and a 12 GHz oscilloscope (Tektronix TDS6124C), in the same cryogen free superconducting magnet system, were used. In these measurements, voltage pulses of 200 ns duration (duty cycle 10^{-4}) were applied along the length of the sample up to a maximum electric field of $F = 260$ kV m^{-1}.

3. Results and discussion

The temperature and electric field dependence of the Hall mobility in the $Al_{0.25}Ga_{0.75}N/AlN/GaN$ heterostructure is plotted in Fig. 1. The Hall mobility of electrons in the $Al_{0.25}Ga_{0.75}N/AlN/GaN$ heterostructure increases monotonically with decreasing temperature, and the electric field from room temperature begins to level off at about 100 K and saturates at about 20 K (see Fig. 1). This behavior reflects the 2D character of the electrons in the channel [19–21].

Fig. 2 shows typical examples of the magnetoresistance $R_{xx}(B)$ measured at different temperatures and an applied electric field for $Al_{0.25}Ga_{0.75}N/AlN/GaN$ heterostructures. SdH oscillations are clearly visible over the magnetic field range between $B = 5$ and 11 T. No higher harmonics are apparent in the oscillations. It is also evident that the oscillatory effect is superimposed on a monotonically increasing component, which occurs as a result of positive magnetoresistance in the barriers [7,19]. This may affect the accuracy of the determination of oscillation amplitude, particularly at elevated temperatures. Therefore, in order to exclude the effects of the background magnetoresistance (R_b) and to extract the SdH oscillations, we used the negative second derivative of the raw magnetoresistance data with respect to the magnetic field, i.e. $(-\partial^2 R_{xx}/\partial B^2)$ [7,19,22,23]. The oscillations in the second derivative of magnetoresistance have well defined envelopes and are symmetrical about the horizontal line as shown in Fig. 3. The double-differentiation technique does not change the peak position or the period of the oscillations [19,23].

In modulation-doped structures, where a highly-degenerate electron gas exists, the variations of the amplitude of the SdH oscillations with an applied electric field and lattice temperature can be used in the determination of the power loss-electron temperature characteristics. The sample used in the present study is degenerate so that the reduced Fermi energy $E_F-E_1/k_B T > 1$, even at electron temperatures of approximately 30 K, which is well above the range of temperatures considered here. Therefore, we employed the SdH oscillations technique in our investigations. The thermal damping of the
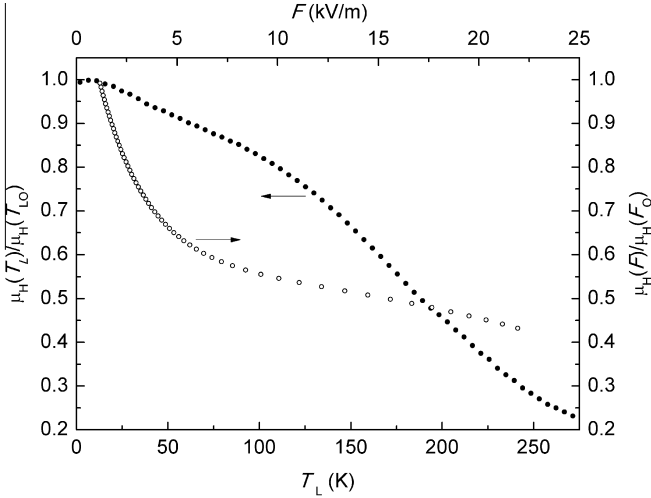
Fig. 1. Temperature and electric field dependence of the Hall mobility (μ_H) of electrons in the $Al_{0.25}Ga_{0.75}N/AlN/GaN$ heterostructure.

amplitude of the SdH oscillations is, therefore, determined by the temperature, magnetic field, and effective mass via [7,19,22–26]:

$$\frac{A(T,B_n)}{A(T_0,B_n)} = \frac{T \cdot \sin h(2\pi^2 k_B m^* T_0/\hbar e B_n)}{T_0 \cdot \sin h(2\pi^2 k_B m^* T/\hbar e B_n)}, \tag{1}$$

where m^*, k_B, $\hbar$ ($=h/2\pi$), e, $A(T,B_n)$, $A(T_0,B_n)$, are the electron effective mass, Boltzmann's constant, Planck's constant, electron charge, amplitudes of the oscillation peaks observed at a magnetic field B_n and at temperatures T and T_0, respectively. In the derivation of Eq. (1) the quantum lifetime of electrons is assumed to be independent of temperature and the effects of higher harmonics are neglected [5–7]. The relative amplitude $A(T,B_n)/A(T_0,B_n)$ decreases with increasing temperature (Fig. 4(a)) in accordance with the usual thermal damping factor [5–7].

Assuming that the change in the SdH amplitude with an applied electric field can be described in terms of electric-field induced electron heating, the temperature T in Eq. (1) can be replaced by the electron temperature T_e. Therefore, T_e can be determined by comparing the relative amplitudes of the SdH oscillations measured as functions of the lattice temperature ($T = T_L$) and the applied electric field (F) using [5–7]:

$$\left[\frac{A(T_L,B_n)}{A(T_{LO},B_n)}\right]_{F=F_0} = \left[\frac{A(F,B_n)}{A(F_0,B_n)}\right]_{T_L=T_{LO}}. \tag{2}$$

Here, $A(F,B_n)$ and $A(F_0,B_n)$ are the amplitudes of the oscillation peaks observed at a magnetic field B_n and at electric fields F and F_0, respectively. In order to obtain the electron temperature from the lattice temperature and electric-field dependencies of the amplitude of the SdH oscillations, the quantum lifetime has to be independent of both the lattice temperature and the applied electric field. Fig. 4(b) shows the amplitudes of the SdH oscillations, normalized as described by Eq. (1), as functions of F for the $Al_{0.25}Ga_{0.75}N/AlN/GaN$ heterostructure sample. In Fig. 4, only the relative amplitudes at a given magnetic field B_n are shown for clarity. A similar analysis made for all the SdH peaks observed in the magnetic field range from 5 to 11 T has established that the relative amplitudes of SdH oscillations (and hence the electron temperatures) in our samples are essentially independent of a magnetic field. This indicates that the magnetic field used in our experiments does not significantly alter the energy relaxation processes of hot electrons.
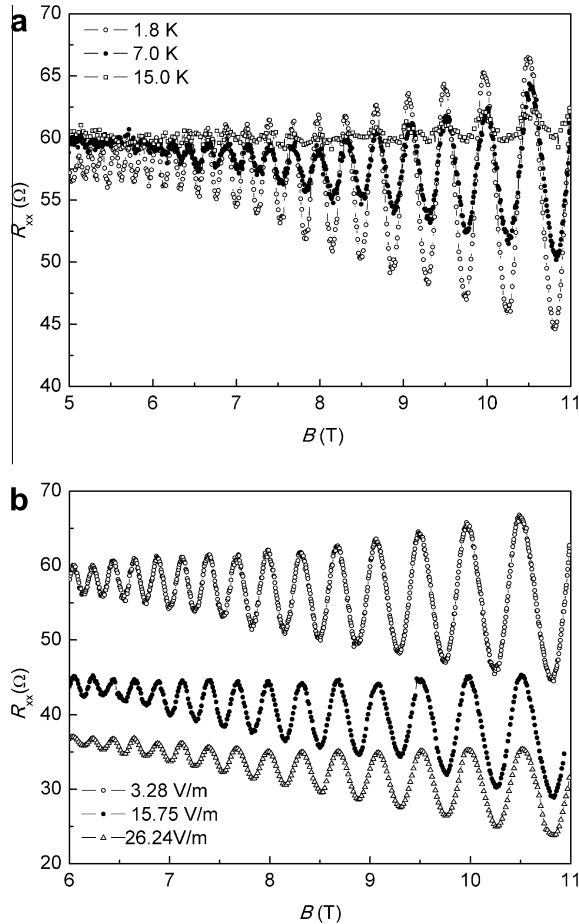
Fig. 2. Experimental results showing the effects of (a) temperature and (b) applied electric field on the magnetoresistance $R_{xx}(B)$ measured for the $Al_{0.25}Ga_{0.75}N/AlN/GaN$ heterostructure sample.

Electron temperatures (T_e) for the $Al_{0.25}Ga_{0.75}N/AlN/GaN$ heterostructure sample, as obtained by directly comparing the curves similar to those in Fig. 4(a), are plotted as a function of the applied electric field in Fig. 4(b). The SdH oscillations measured for the $Al_{0.25}Ga_{0.75}N/AlN/GaN$ heterostructure sample decrease rapidly with increasing the applied electric field. The electron temperature determined for this sample rises quickly with increasing F (Fig. 5(a)).

In mobility comparison methods, the electric field dependent electron temperature can be determined by comparing the relative amplitudes of the mobilities measured as functions of the lattice temperature ($T = T_L$) and the applied electric field (F) using [5,6,10]:

$$\left[\frac{\mu_H(T_L)}{\mu_H(T_{LO})}\right]_{F=F_0} = \left[\frac{\mu_H(F)}{\mu_H(F_0)}\right]_{T_L=T_{LO}}. \tag{3}$$

In order to obtain the electron temperature from the lattice temperature and electric-field dependencies of the amplitude of the mobility, the carrier concentration has to be independent of both the lattice temperature and the applied electric field and intersubband transition has to be forbidden. Electron temperatures (T_e) for the $Al_{0.25}Ga_{0.75}N/AlN/GaN$ heterostructure sample as obtained by directly comparing the mobility curves similar to those in Fig. 1, are plotted as a function of the ap-
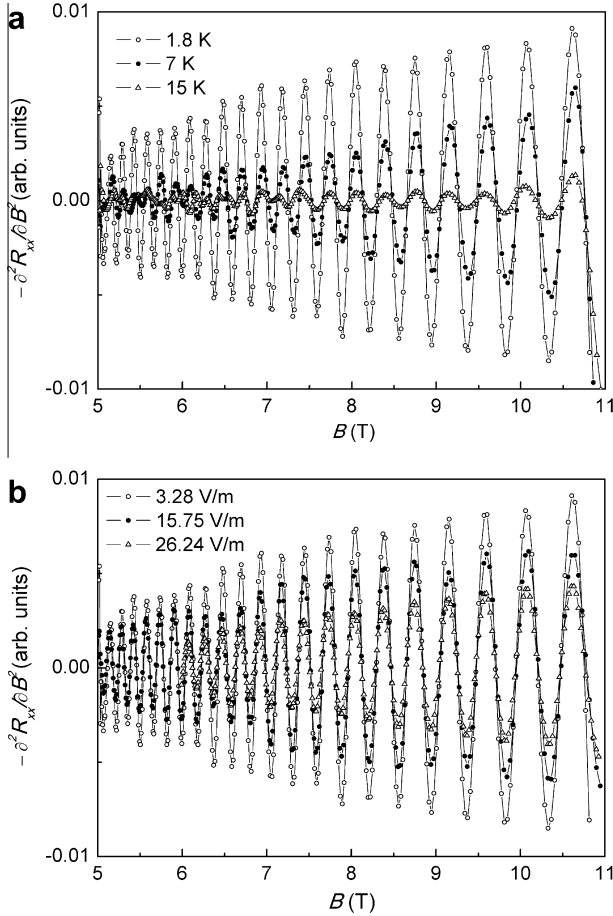
Fig. 3. The effects of temperature (a) and applied electric fields (b) on the SdH oscillations arising from the electrons in the subband, as extracted from the $R_{xx}(B)$ data for the $Al_{0.25}Ga_{0.75}N/AlN/GaN$ heterostructure sample (shown in Fig. 2). The full curves through the experimental data points are intended as a guide. The double differentiation removes the background magnetoresistance without affecting the position and the amplitudes of the oscillatory component.

plied electric field in Fig. 5(b). Electron temperature rises above the lattice temperature at electric fields of around $F = 1$ kV m^{-1}. The maximum electron temperature reached in the experiments at $F > 25$ kV m^{-1} is $T_e = 200$ K.

In the steady state, the power loss from hot electrons by the emission of acoustic phonons is equal to the power supplied by the applied electric field, which can be calculated using the energy balance equation [5,6]:

$$P = e\mu_t F^2, \tag{4}$$

where P and μ_t are the energy loss (or energy supply) rate per electron and transport mobility, respectively. We used the transport mobility (μ_t) as Hall mobility (μ_H) determined from temperature/electric field dependent classical Hall Effect measurements. The power loss per electron versus electron temperature determined both from the SdH measurements and Hall mobility measurements is plotted in Fig. 6.

The electron temperature dependence of the power loss was found to be different than the previous reports on energy relaxation by hot electrons [12–15] in GaN/AlGaN heterojunctions. Since the
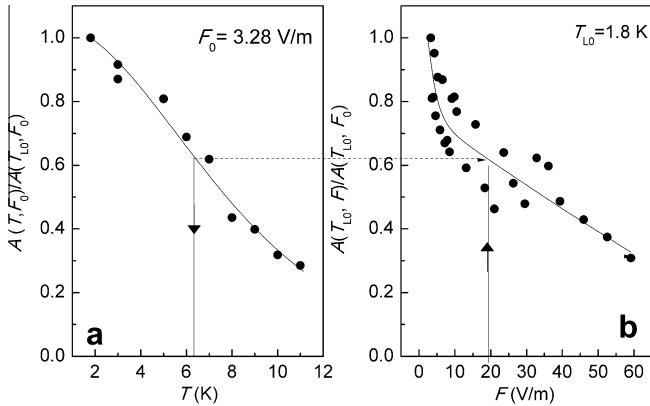
Fig. 4. (a) Temperature and (b) electric-field dependencies of the normalized amplitude of the oscillation peak at B_n measured in an $Al_{0.25}Ga_{0.75}N/AlN/GaN$ heterostructure. The data points represented by the full circles correspond to the SdH oscillations arising from the electrons in the subband. The full curve in (a) is the best fit of Eq. (1) to the experimental data. The full curve in (b) is intended as a guide.
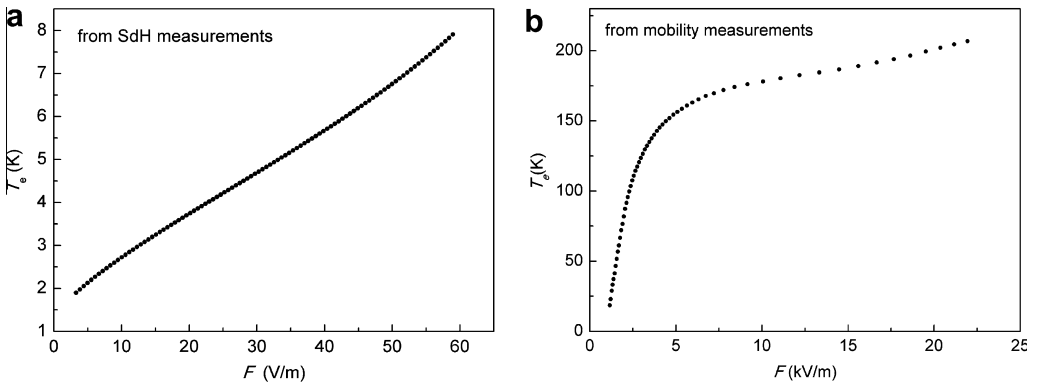

Fig. 5. Electron temperature (T_e) versus the applied electric field (F) for $Al_{0.25}Ga_{0.75}N/AlN/GaN$ heterostructures. The full curves through the experimental data points are intended as a guide.

layer structures and doping parameters of all the investigated samples are identical, the observed variations in power loss may be associated with the differences in the mobility of the samples (see Eq. (4)).

The variation of the power loss per electron with electron temperature in the acoustic phonon regime has been often approximated by the relationship:

$$P_{exp} = A(T_e^{\gamma} - T_{LO}^{\gamma}), \tag{5}$$

where A is the proportionality constant, which depends on the elastic moduli of the matrix, the coupling constants and the 2D carrier density. Theoretical calculations of the acoustic phonon assisted energy loss rates of hot electrons in a 2D electron gas of single-subband occupancy predict $\gamma = 1$ at high temperatures (when Maxwell–Boltzmann statistics is applicable and equipartition is assumed) and $\gamma = 3$ (unscreened piezoelectric scattering), $\gamma = 5$ (unscreened deformation potential and heavily-screened piezoelectric scatterings) and $\gamma = 7$ (heavily-screened deformation potential scattering) at low temperatures (see for instance Ref. [2]). We found the exponent 2.50 by fitting Eq. (5) to the experimental data (Fig. 6(a)). In all cases, a constant value for the exponent γ is obtained over the whole temperature range. This indicates that the experiments were carried out in the low-tempera-
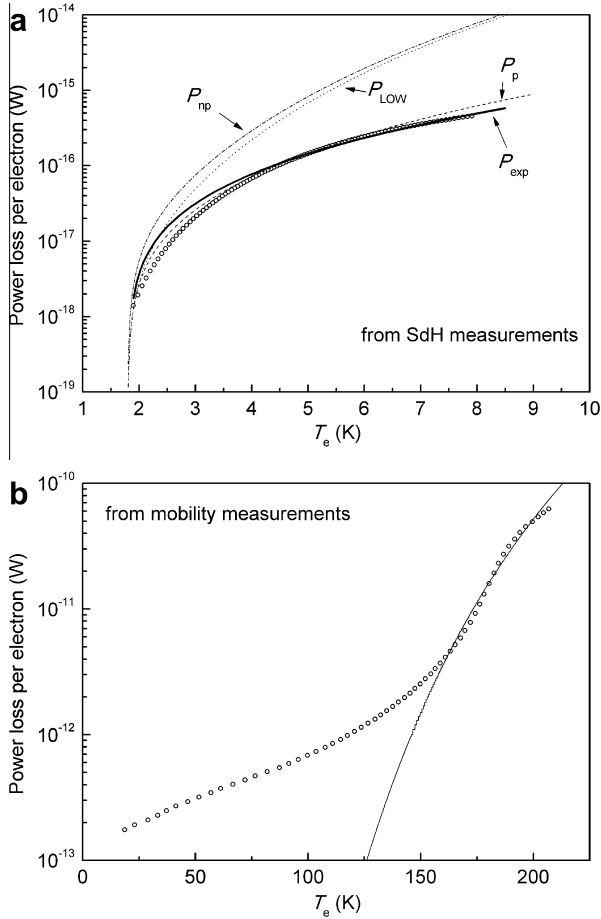
Fig. 6. (a) Electron temperature dependence of power loss per electron determined from SdH measurements. The full circles correspond to the experimental data. The dashed, dotted, dash dotted, and full curves correspond to the power loss calculated using Eqs. (5), (7)–(9) respectively. (b) Electron temperature dependence of power loss per electron determined from Hall mobility measurements. The full curves correspond to the power loss calculated using Eq. (15).

ture regime and that the energy relaxation is due to acoustic phonon emission via mixed unscreened piezoelectric and deformation potential interactions.

We have also fitted the experimental $P(T_e)$ data to the theoretically derived analytical expressions for power loss. At low temperatures, the carrier distribution is often degenerate, and Pauli exclusion is important in limiting the scattering that is allowed [2,27–30]. In the 2D calculations, the scattering by the absorption of acoustic phonons was neglected and only spontaneous emission was considered to be important, the infinite-well approximation was used in the extreme quantum limit, and the phonons were assumed to be bulk phonons [2,7]. The power loss from a degenerate electron gas due to scattering by acoustic phonons has been calculated [2,28,30] in two temperature regimes: (i) the low-temperature (Bloch–Grüneisen) regime, where the electron temperature the $T_e \ll T_e^c$, and (ii) the high-temperature regime, where $T_e \gg T_e^c$, hence the critical electron temperature is given [30] by:

$$T_e^c = \frac{[8m^* V_s^2 (E_F - E_1)]^{1/2}}{k_B},$$

(6)

where E_F, E_1, V_S are the Fermi energy, first-subband energy, and sound velocity, respectively. The regime between these two temperature limits is called the intermediate regime [2,7]. The critical

electron temperature of the investigated $Al_{0.25}Ga_{0.75}N/AlN/GaN$ heterostructure calculated using the values (Table 1) determined experimentally for the effective mass and Fermi energy of 2D electrons is found to be approximately 67 K, indicating that the SdH experiments were carried out in the low-temperature regime.

At low temperatures, the Fermi gas has a sharp boundary curve and consequently momentum changes that involve the emission of an acoustic phonon of energy much greater than $k_B T_e$ are significantly hindered. Hence, only small-angle scattering is allowed at very low temperatures [29].

In the low-temperature regime, the energy-loss rate of a 2D electron gas is characterized by the dependencies $P_{np} \propto (T_e^5 - T_{LO}^5)$ for deformation potential (nonpolar acoustic) scattering and $P_p \propto (T_e^3 - T_{LO}^3)$ for piezoelectric (polar acoustic) scattering [29,30]. Therefore, the total energy-loss rate of a 2D electron gas, in the low-temperature regime, can be represented [2,7] by:

$$P = P_{np} + P_p, \tag{7}$$

where

$$P_{np} = \frac{6\Xi^2 m^{*2} L_z}{\pi^3 \rho \hbar^7 V_S^4 N_{2D}}[(k_B T_e)^5 - (k_B T_L)^5], \tag{8}$$

and

$$P_p = \frac{e^2 K_{av}^2 m^{*2}}{2\pi^2 \varepsilon \hbar^5 k_F N_{2D}}[(k_B T_e)^3 - (k_B T_L)^3]. \tag{9}$$

Here, Ξ is the acoustic deformation potential, ρ is the mass density, ε_s is the static permittivity, and $k_F = [2\pi N_{2D}]^{1/2}$ is the Fermi wave vector of 2D electrons in which N_{2D} is the 2D carrier density. The average electromechanical coupling constant K_{av}^2 for cubic crystal is given [7] by:

$$K_{av}^2 = \frac{e_{14}^2}{\varepsilon}\left(\frac{12}{35C_L} + \frac{16}{35C_T}\right). \tag{10}$$

Here, e_{14} is the piezoelectric stress constant, and C_L and C_T are the average longitudinal and transverse elastic constants, given [31] in terms of the components of the elastic stiffness constants C_{ij} by:

$$C_L = C_{11} + \frac{2}{5}(C_{12} + C_{44} - C_{11}) \tag{11}$$

and

$$C_T = C_{44} - \frac{1}{5}(C_{12} + 2C_{44} - C_{11}). \tag{12}$$

Table 1
Material parameters of the $Al_{0.25}Ga_{0.75}N/AlN/GaN$ heterostructure used in the calculation (Refs. [15,21,32–35]).

Parameter	Value
2D carrier density, N_{2D} (10^{16} m^{-2})	9×10^{16}
Effective mass, m^* (m$_0$)	0.206
Fermi energy, $E_F - E_1$ (meV)	92.3
γ	2.50
A (eV s^{-1} K$^{-\gamma}$)	2.79×10^{-18}
Acoustic deformation potential, Ξ (eV)	−7.7
LO phonon energy, $\hbar\omega_{LO}$ (eV)	91.2
Static permittivity constant, ε_s (ε_0)	10
High frequency dielectric constant, ε_∞ (ε_0)	5.35
C_{11} (GPa)	373
C_{12} (GPa)	141
C_{44} (GPa)	94
e_{14} (C/m^2)	0.375
Mass density, ρ (kg m^{-3})	6150
Sound velocity, V_s (m/s)	6560

We assumed that the effective well width (L_Z) of the potential well at the $Al_{0.25}Ga_{0.75}N/AlN/GaN$ interface is $L_Z \approx 2\pi/k_F$ [10].

The power loss, as given by Eq. (7), has been calculated using the values (Table 1) determined experimentally [21,32] for the effective mass, longitudinal optical phonon energy, carrier density and Fermi energy of 2D electrons in the $Al_{0.25}Ga_{0.75}N/AlN/GaN$ heterostructure sample; other parameters are taken from the literature [15,33–35].

Although the non-polar component of analytical expression of the power loss (Eq. (8)) and the total power loss (Eq. (7)) do not offer a satisfactory fit to the experimental data, the polar component of the analytical expression of the power loss (Eq. (9)) is in good agreement with the experimental power loss data for the $Al_{0.25}Ga_{0.75}N/AlN/GaN$ heterostructure sample. These trends remain at all electron temperatures in the range of 1.8–8 K. This result is also in accord with the fitting outcome of the Eq. (5) and other researchers' results in AlGaN/GaN heterojunctions [12–15].

At high temperatures, the electrons relax emitting LO phonons and thereby reduce in energy and momentum. An expression for the power loss due to optical phonon emission and absorption can be written [10,11] in the form:

$$P = \frac{\hbar\omega_{LO}}{\langle\tau_E\rangle}\left[\exp\left(-\frac{\hbar\omega_{LO}}{k_B T_e}\right) - \exp\left(-\frac{\hbar\omega_{LO}}{k_B T_L}\right)\right], \tag{13}$$

where $\langle\tau_E\rangle$ is the electron–phonon scattering time for the e–LO interaction [36]:

$$\langle\tau_E\rangle = \frac{4\pi\varepsilon^*\varepsilon_0\hbar}{3e^2 N}\left(\frac{2\hbar}{m^*\omega_{LO}(1 + \hbar\omega_{LO}/E_g)}\right)^{1/2}\frac{I_2(\gamma)}{I_1(\gamma)}, \tag{14}$$

where

$$\frac{1}{\varepsilon^*} = \frac{1}{\varepsilon_\infty} - \frac{1}{\varepsilon_s} \tag{15}$$

with ε_∞ is the high frequency dielectric constant, $N = 1/(e^{\hbar\omega_{LO}/k_B T} - 1)$ is the Planck distribution function, E_g is the band gap energy of GaN, and

$$I_1(\gamma) = \int_0^\infty (1 + 2\gamma x)\sqrt{x(1 + \gamma x)}\exp(-x)dx, \tag{16}$$

$$I_2(\gamma) = \int_0^\infty [x(1 + \gamma x)]^{3/2}(1 + 2\gamma x)^{-1}\exp(-x)dx, \tag{17}$$

where

$$\gamma = \frac{k_B T}{E_g}. \tag{18}$$

The power loss due to optical phonon emission was calculated using the theoretical expression given in Eq. (13) with the material parameters in Table 1. The results obtained for the temperature dependences of power loss are also presented in Fig. 6(b). Although the calculated power loss does not offer a satisfactory fit to the experimental data in the electron temperature range between 20 and 150 K, it fits reasonably well to the experimental data for $T_e > 150$ K. From the temperature dependence of the Hall mobility compared with the calculated various electron mobility was shown that the mobility of electrons in $Al_{0.25}Ga_{0.75}N/AlN/GaN$ heterostructures is determined by mixed interface roughness scattering and polar optical phonon scattering in the temperature range between 20 and 150 K [21]. Therefore, it is clear that the addition of the other scattering time together with the optical phonon scattering time is necessary in the definition of the electron–phonon scattering time (Eq. (14)).

The energy relaxation time (τ_E) in the acoustic-phonon regime can be obtained from the power loss measurements using [2]:

$$P = \frac{\langle\hbar\omega\rangle}{\tau_E}\frac{(k_B T_e - k_B T_{LO})}{k_B T_e}, \tag{19}$$

where $\langle\hbar\omega\rangle = \sqrt{2}\hbar V_S k_F$ is the acoustic-phonon energy averaged over the Fermi surface. Fig. 7(a) shows the energy relaxation time as a function of the electron temperature for the $Al_{0.25}Ga_{0.75}N/AlN/GaN$
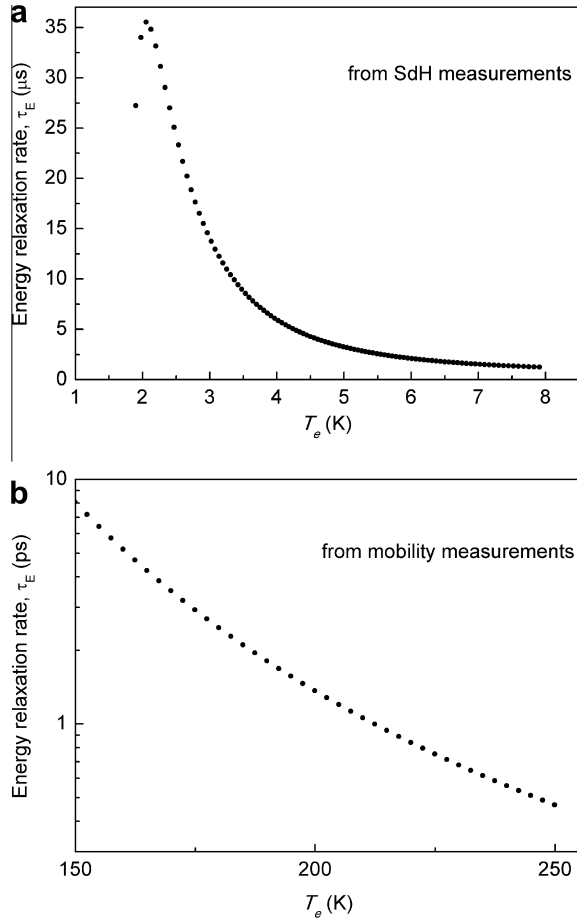
Fig. 7. Energy relaxation time (τ_E) versus T_e obtained from (a) SdH measurements and (b) mobility measurements for the $Al_{0.25}Ga_{0.75}N/AlN/GaN$ heterostructure.

heterostructure sample studied. Such large values of T_E indicate that the energy loss mechanism in this temperature range is not very efficient and leads to the rapid rise of the electron temperature when the input power is increased (see Fig. 6(a)). However, as can be seen in Fig. 7(a), the energy relaxation due to acoustic phonons accelerates at higher electron temperatures.

The energy relaxation time (τ_E) in the optical-phonon regime, $T_e > 150$ K, can be obtained from using Eq. (14). The energy relaxation time of hot electrons in the $Al_{0.25}Ga_{0.75}N/AlN/GaN$ heterostructure decreases monotonically with increasing temperature from 150 K to room temperature (Fig. 7(b)). At 250 K, the energy relaxation time is $\tau_E = 0.47$ ps. Tsen et al. [17] investigated the carrier dependence of the energy relaxation time in GaN grown on sapphire substrate by using subpicosecond time-resolved Raman measurements at room temperature. They found that the energy relaxation time decreased from 2.5 to 0.35 ps when the carrier density increased from 10^{16} to 2×10^{19} cm^{-3}. The τ_E value obtained from mobility measurements at 250 K is in reasonable agreement with the results of Raman spectroscopy [17] and what was obtained by other research groups [4,10,17,37].

4. Conclusion

The energy-loss rates, in the acoustic phonon regime, of 2D electrons in the $Al_{0.25}Ga_{0.75}N/AlN/GaN$ heterostructure were investigated using SdH effect measurements. The experimental results were

compared with the predictions of the current theoretical models for power loss in semiconductors. We found agreement between the experimental results and theory. Whereas, at low temperatures, the energy relaxation of electrons is due to acoustic phonon emission via unscreened piezoelectric interaction, at high temperatures the energy relaxation of electrons is due to optical phonon emission. The energy relaxation time of hot electrons in the $Al_{0.25}Ga_{0.75}N/AlN/GaN$ heterostructure decreases monotonically with increasing temperature from 1.8 K to room temperature.

Acknowledgments

References

[1] H. Morkoc, Handbook of Nitride Semiconductors and Devices, vols. I–III, Wiley-VCH, Weinheim, 2008.
[2] B.K. Ridley, Rep. Prog. Phys. 54 (1991) 169.
[3] S. Mazzucato, M.C. Arikan, N. Balkan, B.K. Ridley, N. Zakhleniuk, R.J. Shealy, B. Schaff, Physica B 314 (2002) 55.
[4] A. Matulionis, J. Liberis, E. Sermuksnis, J. Xei, J.H. Leach, M. Wu, H. Morkoc, Semicond. Sci. Technol. 23 (2008) 075048.
[5] H. Kahlert, G. Bauer, Phys. Status Solidi B 46 (1971) 535.
[6] G. Bauer, H. Kahlert, Phys. Rev. B 5 (1972) 566.
[7] N. Balkan, H. Celik, A.J. Vickers, M. Cankurtaran, Phys. Rev. B 52 (1995) 17210.
[8] E. Tiras, M. Cankurtaran, H. Celik, N. Balkan, Phys. Rev. B 64 (2001) 085301.
[9] M.C. Arikan, A. Straw, N. Balkan, J. Appl. Phys. 74 (1993) 6261.
[10] N. Balkan, M.C. Arikan, S. Gokten, V. Tilak, B. Schaff, J. Phys.: Condens. Matter 14 (2002) 3457.
[11] A. Ilgaz, S. Gokten, R. Tulek, A. Teke, S. Ozcelik, E. Ozbay, Eur. Phys. J. Appl. Phys. 55 (2011) 30102.
[12] K.J. Lee, J.J. Harris, A.J. Kent, T. Wang, S. Sakai, D.K. Maude, J.C. Portal, Appl. Phys. Lett. 78 (2001) 2893.
[13] N.M. Stanton, A.J. Kent, S.A. Cavill, A.V. Akimov, K.J. Lee, J.H. Harris, T. Wang, S. Sakai, Phys. Status Solidi B 228 (2001) 607.
[14] C.E. Martinez, N.M. Stanton, A.J. Kent, M.L. Williams, I. Harrison, H. Tang, J.B. Webb, J.A. Bardwell, Semicond. Sci. Technol. 21 (2006) 1580.
[15] H. Cheng, N. Biyikli, J. Xie, C. Kurdak, H. Morkoc, J. Appl. Phys. 106 (2009) 103702.
[16] A. Matulionis, J. Phys.: Condens. Matter 21 (2009) 174203.
[17] K.T. Tsen, J.G. Kiang, D.K. Ferry, H. Morkoc, Appl. Phys. Lett. 89 (2006) 112111.
[18] S.B. Lisesivdin, S. Demirezen, M.D. Caliskan, A. Yıldız, M. Kasap, S. Ozcelik, E. Ozbay, Semicond. Sci. Technol. 23 (2008) 095008.
[19] E. Tiras, M. Cankurtaran, H. Celik, A.B. Thoms, N. Balkan, Superlattices Microstruct. 29 (2001) 147.
[20] S. Altinoz, E. Tiras, A. Bayrakli, H. Celik, M. Cankurtaran, N. Balkan, Phys. Status Solidi A 182 (2000) 717.
[21] O. Celik, E. Tiras, S. Ardali, S.B. Lisesivdin, E. Ozbay, Cent. Eur. J. Phys. (accepted).
[22] H. Celik, M. Cankurtaran, A. Bayrakli, E. Tiras, N. Balkan, Semicond. Sci. Technol. 12 (1997) 389.
[23] E. Tiras, N. Balkan, S. Ardali, M. Gunes, F. Fontaine, A. Arnoult, Philos. Mag. 91 (2011) 628.
[24] D.G. Seiler, A.E. Stephens, in: G. Landwehr, E.I. Rashba (Eds.), Landau Level Spectroscopy, vol. 2, North-Holland, Amsterdam, 1991, p. 1031.
[25] S.B. Lisesivdin, N. Balkan, O. Makarovsky, A. Patane, A. Yildiz, M.D. Caliskan, M. Kasap, S. Ozcelik, E. Ozbay, J. Appl. Phys. 105 (2009) 093701.
[26] H. Celik, M. Cankurtaran, A. Bayrakli, E. Tiras, N. Balkan, Phys. Status Solidi B 207 (1998) 139.
[27] P.J. Price, J. Appl. Phys. 53 (1982) 6863.
[28] S.D. Sarma, J.K. Jain, R. Jalabert, Phys. Rev. B 37 (1989) 6290.
[29] V. Karpus, Fiz. Tekh. Poluprovodn. 22 (1988) 439, [Sov. Phys. Semicond. 22 (1988) 268].
[30] A.M. Kreshchuk, M.Y. Martisov, T.A. Polyanskaya, I.G. Savel'ev, I.I. Saidashev, A.Y. Shik, Y.V. Shmartsev, Fiz. Tekh. Poluprovodn. 22 (1988) 604, [Sov. Phys. Semicond. 22 (1988) 377].
[31] M.P. Vaughan, B.K. Ridley, Phys. Rev. B 72 (2005) 075211.
[32] O. Celik, E. Tiras, S. Ardali, S.B. Lisesivdin, E. Ozbay, Phys. Status Solidi C 8 (2011) 1625.
[33] W.J. Fan, S.F. Yoon, J. Appl. Phys. 90 (2001) 843.
[34] S. Adachi, Properties of Semiconductor Alloys: Group IV, III–V and II–VI semiconductors, first ed., John Wiley & Sons Ltd, United Kingdom, 2009.
[35] A.D. Bykhovski, V.V. Kaminski, M.S. Shur, Q.C. Chen, M.A. Khan, Appl. Phys. Lett. 68 (1996) 818.
[36] L. Hsu, W. Walukievicz, Phys. Rev. B 56 (1997) 1520.
[37] A. Matulionis, J. Liberis, L. Ardaravicius, J. Smart, D. Pavlidis, S. Hubbard, L.F. Eastman, Int. J. High Speed Electron. Syst. 12 (2002) 459.